Impact of Silk-Ionomer Encapsulation on Immune Cell Mechanical Properties and Viability

Udathari Kumarasinghe¹, Onur Hasturk², Brook Wang², Sara Rudolph², Ying Chen², David L. Kaplan²*, Cristian Staii¹*.*

¹Department of Physics and Astronomy, Tufts University, Medford, MA 02155, USA

²Department of Biomedical Engineering, Tufts University, Medford, MA 02155, USA

*Corresponding authors: ying.chen@tufts.edu, david.kaplan@tufts.edu, cristian.staii@tufts.edu

KEYWORDS: Cell encapsulation, silk ionomers, layer-by-layer assembly, Atomic Force Microscopy, ell viability

ABSTRACT

Encapsulation of single cells is a powerful technique used in various fields, such as regenerative medicine, drug delivery, tissue regeneration, cell-based therapies, and biotechnology. It offers a method to protect cells by providing cytocompatible coatings to strengthen cells against mechanical and environmental perturbations. Silk fibroin, derived from the silkworm Bombyx mori, is a promising protein biomaterial for cell encapsulation due to the cytocompatibility and capacity to maintain cell functionality. Here, THP-1 cells, a human leukemia monocytic cell line, were encapsulated with chemically modified silk polyelectrolytes through electrostatic layer-by-layer deposition. The effectiveness of the silk nanocoating was assessed using scanning electron microscopy (SEM) and confocal microscopy and on cell viability and proliferation by Alamar Blue assay and live/dead staining. An analysis of the mechanical properties of the encapsulated cells was conducted using atomic force microscopy (AFM) nanoindentation to measure elasticity maps and cellular stiffness. After the cells were encapsulated in silk, an increase in their stiffness was observed. Based on this observation, we developed a mechanical predictive model to estimate the variations in stiffness in relation to the thickness of the coating. By tuning the cellular assembly and biomechanics, these encapsulations promote systems that protect cells during biomaterial deposition or processing in general.

1. INTRODUCTION

Encapsulation of cells has been used over recent decades in various fields such as biotechnology, regenerative medicine, and drug delivery ¹⁻⁸. This technique involves modifying the cell surface by applying biomaterial film coatings onto cell membranes, thus, enclosing living cells within a protective and cytocompatible barrier while retaining their functionality and viability. Encapsulation of mammalian cells has been widely reported as a method to overcome challenges in many applications, as the cells are otherwise vulnerable to fluctuations in their surrounding environment due to the absence of structural support, especially in harsh and hostile conditions. Applications including cell therapy, tissue engineering, 3D printing, and transplantation of cells and tissues often require the ex vivo manipulation and handling of cells. Mechanical forces such as shear stress and extensional forces are unavoidable environmental perturbations that cells encounter during these processes, leading to damage to the plasma membrane and subsequent leakage of cytosol components and cell death ⁹⁻¹². Hence, encapsulation of individual cells using biocompatible materials has emerged as a promising approach to provide protection against various mechanical interactions between the cells and the external environment. This versatile technique can accommodate primary cells, stem cells and genetically modified cells, for different applications, expanding the possibilities for diverse research fields such as tissue regeneration, cell-based therapies, cell printing, and cell-based biosensors ^{2, 7-8, 13-16}.

Encapsulation of individual cells has been achieved through several approaches, including coacervation techniques, binding of biopolymers to surface receptors, 3D bioprinting, hydrogel encapsulation, and *in situ* polymerization ^{6, 14}. Among the diverse range of cell encapsulation techniques, electrostatic Layer-by-Layer (LbL) deposition is the simplest, most versatile and

commonly used technique, as it allows for precise control over the thickness and properties of the encapsulating layers. This technique involves the sequential deposition of alternating layers of biocompatible polyelectrolytes onto cell surfaces through self-assembly via electrostatic forces ¹⁵. Various mammalian cells have been successfully encapsulated through LbL deposition using different natural or synthetic coating materials ¹⁶⁻²³. Even though these materials are successfully deposited on the cell surface, many can be cytotoxic to the mammalian cells, impacting their cell proliferation, differentiation, and function. Additionally, many of these materials do not provide mechanical rigidity, which hinders their utility ^{1, 24-25}.

Among numerous candidates for single-cell encapsulation, silk fibroin (SF), a natural protein-based biomaterial derived from Bombyx mori silkworm cocoons, stands out as a promising biomaterial due to its desirable biological and physical properties, including biocompatibility, mild immunogenicity, mechanical properties, manipulability, and biodegradability²⁶⁻²⁷. Additionally, SF preserves cell viability, proliferation, and other vital functionalities after encapsulation while enhancing their stiffness and resistance to external mechanical perturbations ²⁸⁻²⁹. Mechanical properties of SF are promoted by the natural formation of β -sheet crystals where the mechanical characteristics can be tuned by inducing β sheet formation^{26, 30-33}. However, encapsulating cells with pristine SF is challenging as SF has a net negative charge ³⁴, and the membrane resting potential of the cell is usually negative ³⁵⁻³⁶. Silk has been chemically modified by incorporating sufficient net charge to deposit silk through electrostatic LbL to overcome this drawback. By coupling silk fibroin with poly-lysine hydrobromide (PL) and poly-glutamic (PG) acid sodium salts, silk ionomers have been synthesized previously and used for successful encapsulation^{20, 37-39}. However, these coating materials are not compatible with mammalian cells due to their higher charge density, making

them cytotoxic. Recently, we have developed a novel method of synthesis of silk ionomers involving the carboxylation and amination of SF with a lower charge density for the encapsulation of mammalian cells ¹⁵. Utilizing this approach, we have successfully coated adherent mammalian cells, including murine fibroblasts (L929) and human mesenchymal stem cells (hMSCs) with three bilayers of carboxylated and aminated SF and demonstrated the formation of transient, silk-based protein nanoshells that dissociate over time. This process facilitated cell proliferation and underscored the potential for cytocompatible applications.

In the present study, we encapsulated THP-1 cells using our previously developed silk-based ionomers. These ionomers self-assemble through a layer-by-layer technique, creating cytocompatible coatings that enhance cell stiffness¹⁵. The encapsulation of THP-1 cells, a type of suspension blood cell, introduces a novel dimension to our research, as it extends our previous work on the encapsulation of adherent cells to include suspension cells. THP-1 cells, derived from human monocytic cell lines, are capable of differentiating into macrophages or dendriticlike cells, making them an excellent tool for investigating immune responses. Their application is broad, covering research areas such as inflammation, infectious diseases, and immune modulation. Their ease of culture and maintenance highlight their suitability for various experimental designs⁴⁰⁻⁴². These factors collectively prompted us to choose THP-1 cells as our model for the nanocoating study. Encapsulation of immune cells is often utilized in immunotherapy and related experimental applications ⁴³⁻⁴⁶. Such encapsulation can shield immune cells from the host's immune response, particularly in cases where the immune cells are modified or engineered for the survival and functional efficacy of the transplanted or modified cells in experimental and clinical settings. Encapsulating THP-1 cells using silk-based materials makes it possible to create a physical

protective microenvironment for the cells, and to serve as a valuable technique for understanding immune cell biology and developing potential immunotherapeutic approaches.

Mechanical protection from encapsulation can be monitored by measuring the stiffness of living cells after encapsulation. Among the various approaches used to evaluate the stiffness of cells and tissues, Atomic Force Microscope (AFM) – based nanoindentation effectively measures stiffness reliably. Fundamentally, this approach involves indenting a cell with an AFM tip with a specific geometry and measuring the applied force through the deflection of the AFM cantilever (Figure 1). Quantitative measurements of material stiffness can be obtained by fitting the forceindentation curve to the corresponding mechanical model. This technique has been widely used to characterize the mechanical properties of living cells and tissues⁴⁷⁻⁵². Using the AFM nanoindentation technique, we investigated the variation of stiffness of cells after the encapsulation process with different numbers of bilayers. Furthermore, we compared our experimental data for stiffness measured with the AFM with the predictions of a mathematical model based on the Bec/Tonck framework ⁵³. This model describes the stiffness of a composite film/substrate system that mimics our silk-coated cell system and is used to predict the variation of elastic modulus as a function of the thickness of the coating layer. We discuss the fabrication techniques and characterization methods and evaluated the impact of silk encapsulation on cell proliferation and overall viability. By investigating the effect of silk encapsulation on THP-1 cells, this research aims to contribute to the growing body of knowledge in the field of cell encapsulation and highlight the potential of silk-based systems for advancing cell-based therapies and regenerative medicine. Overall, the encapsulation of THP-1 cells using silk holds promise as a strategy to protect and enhance the functionality of these cells, opening up new avenues for therapeutic applications.

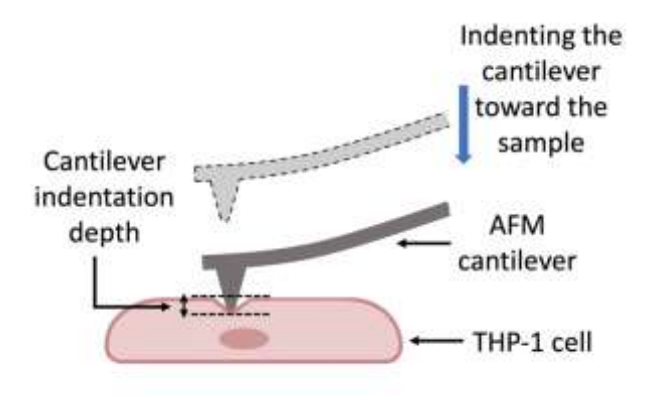


Figure 1. Illustration of AFM nanoindentation. AFM cantilever indents into the cell until the cantilever deflects. The indentation depth of the cantilever and the force applied can be measured to extract the stiffness of the cell.

2. MATERIALS AND METHODS

2.1 Cell culture

THP-1 cells (ATCC, Manassas, VA) were cultured in RPMI 1640 (Gibco, #11875085) with 10% fetal bovine serum (Gibco, #26140079) and 2-mercaptoethanol (0.05 mM) (Gibco, #21985023) in 75 cm² tissue culture flasks at a density of 2×10⁵ viable cells/ml at 37°C in a humidified 5% CO₂ incubator according to the instructions by the manufacturer. Cells were subcultured when cell density reached 8×10⁵ cells/mL and the culture medium was changed every 2 to 3 days.

2.2 Preparation of silk solutions and LbL deposition of silk ionomers on the cell surface Aminated (SF-NH₂) and carboxylated (SF(Y)-COOH) silk solutions were prepared as described by Hasturk et al. ¹⁵. Briefly, *B. mori* silkworm cocoons were degummed to remove sericin protein. Degummed fibers were dried overnight, solubilized in lithium bromide solution (Sigma-

Aldrich, MI, USA), dialyzed against distilled water, and centrifuged twice to remove insoluble particles. For carboxylation, 4-aminobenzoic acid (Sigma-Aldrich, St. Louis, MO) was diazonium-coupled on phenol side chains of tyrosine moieties. For amination, the silk backbone was reacted with ethylenediamine dihydrochloride (EDA, Sigma-Aldrich, St. Louis, MO), in the presence of 1-ethyl-3-(3-(dimethylamino)propyl) carbodiimide (EDC, Sigma-Aldrich, St. Louis, MO), and N-hydroxy succinimide (NHS, Sigma-Aldrich, St. Louis, MO) in 2-(N-Morpholino)ethanesulfonic (MES, Thermo Fisher Scientific, Rockford, IL) buffer. After the reaction, the solution was centrifuged at 9000 rpm at 4 °C for 20 min to remove any insoluble or undesired crosslinking products. The supernatant was then dialyzed extensively against distilled water for 3 days with 6 water changes in dialysis tubing with 3500 Da molecular weight cut-off (MWCO) to remove any unreacted EDA.2HCl (133.02 Da), EDC (191.7 Da), NHS (115.09 Da), or the isourea by-products (~174 Da) of the carbodiimide coupling. After dialysis, the solution was centrifuged again at 9000 rpm at 4 °C for 20 min to remove any potential precipitates and the supernatant was frozen and lyophilized for storage and further use.

The yields of carboxylation and amination were calculated in a previous study done in our lab ¹⁵, as follows: Aminated silk SF-EDA – 88.1%; Carboxylated silk SF(Y)COOH- 29.5%. The silk modification was done on tyrosine (Tyr) residues, which accounts for 5.3 mol% in silk fibroin heavy chain, and we were able to achieve a carboxylation yield of 29.5%. It should be noted that the diazonium coupling is more effective on the tyrosine moieties within the more accessible amorphous regions including the hydrophilic spacer sequences and the non-repetitive N- and C-termini, which account for 20.2% of all tyrosine groups available on fibroin heavy chain (Protein sequence can be accessed on NCBI Genbank, accession #: AAF76983.1). Tyrosine groups located within or at the interface with the semi-crystalline GAGAGY motifs of hydrophobic domains are

less accessible. Thus, a carboxylation yield of 29.5% indicates the conversion of all available tyrosine groups in the amorphous regions and even some of the less accessible ones within or adjacent to the semi-crystalline regions. The previously reported1 increase in the net negative charge from -182.4 ± 54.4 nmol/mg protein on the unmodified silk (120 min degummed) to -414.2 ± 60.8 nmol/mg protein on the tyrosine-carboxylated counterpart together with a decrease in zeta potential from \sim -10 mV to less than -20 mV further confirm the efficiency of carboxylation required for electrostatic deposition.

THP-1 cells were incubated separately in 1, 2 and 5 mg ml-1 solution of aminated silk in 40 mM HEPES buffer supplemented with 5% w/v dextrose and 50 mM NaCl (HD50) at a density of 1×106 cells ml-1 for 1 min with gentle pipetting. Cells were then collected by centrifugation at 2120 rpm for 2 min at 4°C and washed with blank HD50 (without silk solution). Then, to deposit the second layer, cells were incubated in 1,2 and 5 mg ml⁻¹ of carboxylate silk solution for 1 min, centrifuged and washed. These steps were repeated by alternating incubation in aminated and carboxylated silk solutions to deposit the required number of bilayers on the cells.

2.3 Cell viability and metabolic activity

Both encapsulated and control THP-1 cells were stained with a Live/Dead assay kit (Invitrogen, Carlsbad, CA) after seeding and imaged with a BZ-X700 Fluorescence Microscope (Keyence Corp., Itasca, IL) after 30 mins of incubation at 37°C. The percentage cell viability was estimated by analyzing 5 random images from 3 different samples using the live/dead staining macro of ImageJ. Metabolic activity of the cells was monitored at days 0, 2, 4 and 7 by using AlamarBlue viability assay (Invitrogen, Carlsbad, CA) according to the instructions by the manufacturer.

2.4 Confocal Laser Scanning Microscopy (CLSM)

To visualize silk layers deposited on the cell surface, aminated silks were fluorescently labeled using Fluorescein isothiocyanate (FITC, Thermo Fisher Scientific, Rockford, IL)^{3, 15}. FITC was dissolved in dimethyl sulfoxide (DMSO, Sigma-Aldrich, St. Louis, MO) at 10 mg/mL concentration and diluted 4 times with DI water. Diluted FITC solution was added dropwise to the solution of aminated silk solution, then dialyzed, frozen, lyophilized, and stored at -20°C. THP-1 cells were encapsulated with FITC-labeled SF ionomers and visualized using a TCS SP8 microscope from Leica Microsystems (Wetzlar, Germany) at excitation and emission wavelengths of 488 nm/500–540 nm.

2.5 Scanning Electron Microscopy (SEM)

THP-1 cells were prepared for SEM imaging by fixation and dehydration ⁵⁴⁻⁵⁵. THP-1 cells were seeded on trans wells with a pore size of 8 μm at a density of 10⁵ cells cm⁻² and fixed in 1% glutaraldehyde in 1X PBS for 1 hour (hr) at room temperature. After fixation, the sample was gently rinsed once with the same fixed solution and twice with DI water. Then, the samples were dehydrated using a series of 30, 50, 70, 90, and 100% v/v ethanol solutions. Finally, samples were covered with hexamethyldisilazane (HDMS) solution for critical point drying to preserve sample morphology before leaving the samples in the fume hood to air dry. After dehydration, samples were Au-Pd coated under a vacuum and examined under SEM (Zeiss EVO MA10, Germany).

2.6 Atomic Force Microscopy

THP-1 cells were cultured on substrates coated with poly D-lysine (PDL) at a density of 10⁵ cells/ cm² and imaged using an Asylum Research MFP-3D-Bio AFM (Asylum Research, Santa Barbara, CA, USA). For this approach, 4×4 μm maps of individual force vs. indentation curves

on 10 µm² of each THP-1 cell were acquired. In triplicate samples, 5 individual cells were imaged and mapped for each experimental group. We used NanoWorld Pyrex-Nitride triangular (PNP-TR) AFM probes (Asylum Research, Santa Barbara, CA, USA) possessing a force constant of 0.08 N/m. The value of the elastic modulus at each point on the sample was determined by fitting the force vs. indentation curves⁵¹⁻⁵².

3. RESULTS

3.1 Successful encapsulation of THP-1 cells by LBL silk ionomer deposition onto the cell surface

The successful LBL deposition of negatively and positively charged silk layers onto the cell surface was confirmed by imaging THP-1 cells encapsulated with FITC-labeled aminated silk ionomers using confocal microscopy (Figure 2). As expected, the control group that did not undergo the encapsulation procedure exhibited no green GFP signal emission (Figure 2A). The bright-field microscopic image in Figure 2A revealed the large, round, and single-cell morphology of the THP-1 cells, while the experimental groups that received encapsulation with silk at concentrations of 2 mg ml⁻¹ with 3 and 5 bilayers (Figure 2A' and A'', respectively) exhibited bright green fluorescence signals surrounding the cell, indicating the successful encapsulation of the THP-1 cells. The 3D image of cells encapsulated with 3 bilayers shown in Figure 2B indicates that the cell surface is homogeneously covered by silk. The fluorescence, brightfield, and overlay images shown in Figure 2C revealed that every cell in the region observed was encapsulated. Our results suggest that the silk ionomer encapsulation process successfully achieved robust nanocoating around the THP-1 cells.

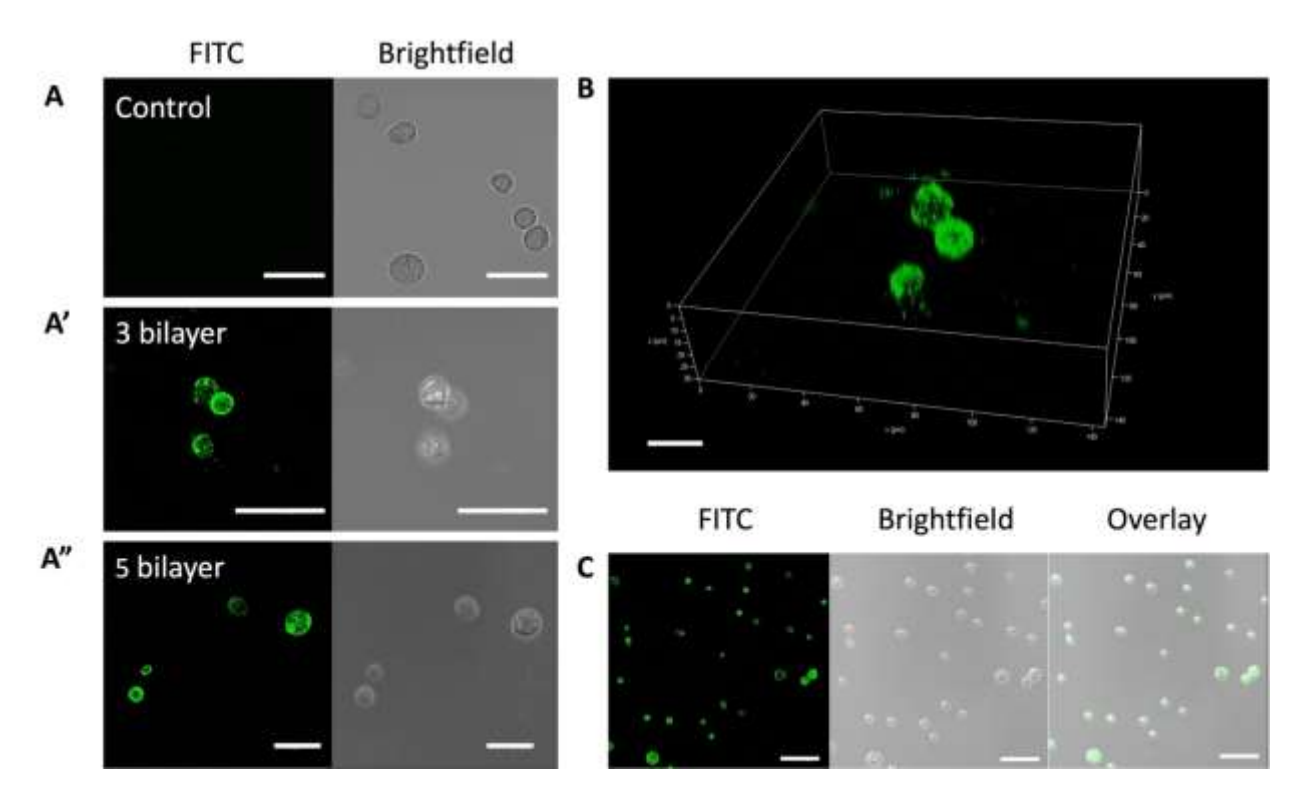


Figure 2. Confocal images of the control and encapsulated THP-1 cells. (A-A") The fluorescence and brightfield images of control, 3-bilayer, and 5-bilayer experimental groups (scale bar:50 μ m). (B) 3D image constructed with z-stack images of encapsulated cells with 3 bilayers of FITC-labeled silk ionomers (scale bar: 20 μ m). (C) The fluorescence, brightfield and overlay images of encapsulated cells with 3 bilayers (scale bar: 100 μ m)

3.2 Characterization of the surface morphology of encapsulated cells

To characterize the surface morphology and further confirm the successful coating achieved through encapsulation, the morphology of both control THP-1 cells and encapsulated cells were visualized by scanning electron microscopy (SEM) after the deposition of three bilayers. This allowed us to examine the surface structure and integrity of the nanocoating around the cells at high resolution. As shown in Figure 3A, the control cells exhibited extracellular projections, in

the form of long filaments on their cell surface, which resembled morphologies observed in normal THP-1 cells⁵⁶⁻⁵⁷. In contrast to the control cells, the encapsulated cells showed a distinct morphology under the SEM. The normal surface structures of the THP-1 cells were masked by the silk bilayers, which formed a uniform coating around the cells (Figure 3B), confirming the successful encapsulation of the cells with silk ionomer. During the imaging process, we noticed the presence of excess silk strands in the surrounding area of the encapsulated cells, which exhibited a similar surface morphology as the encapsulated cells, providing further evidence that the coated layer around the cells was indeed silk ionomer. (Figure. 3C-E).

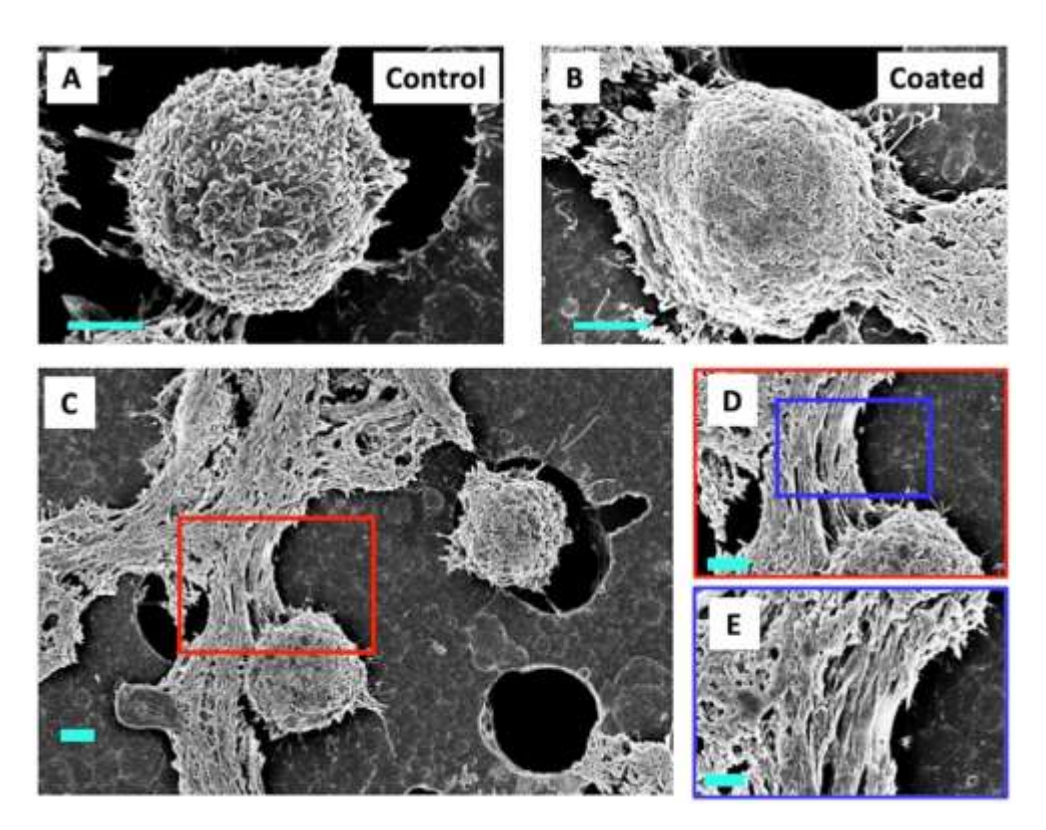


Figure 3. Scanning electron microscopy images of the control and encapsulated THP-1 cells. (A) The controlled cells and (B) encapsulated cells with silk concentration of 2 mg ml⁻¹. Scale bars: 2 μ m (C) Zoomed out image of encapsulated cells, Scale bar: 2 μ m, while (D) is a zoomed image of red box indicated in (C) with scale bars: 2 μ m and (E) is a zoomed image of blue box indicated in (D) showing silk strands, Scale bar: 1 μ m

3.3 Persistence of silk ionomer encapsulation on THP-1 cells with preservation of cell viability and proliferation

To assess the cytotoxic effects of the silk coating on the cells, cell viability was assessed using live/dead staining immediately after encapsulation. Live/dead staining images (Figure 4A) of the uncoated control and experimental groups were used to quantify cell viability (Figure 4B). Herein, we established a control group that underwent the encapsulation process using blank

HD50 instead of silk, where the number of cycles of centrifugation required for encapsulation varied depending on the number of bilayers that we intended to encapsulate (1,2 and 3 bilayers). Live/dead staining images and the quantification of cell viability of the control spin group showed that the number of centrifugations did not significantly affect cell viability, whereas, for all control groups, cell viability was above 96%. The experimental groups where the cells were encapsulated with silk at 1 and 2 mg ml⁻¹ concentrations with 3 and 5 bilayers exhibited some cytotoxicity. This effect increased when the concentration of silk used for encapsulation went from 1 to 2 mg ml⁻¹, regardless of the number of bilayers. However, the impact was minimal, as ~80% of the encapsulated cells still survived, which was not significantly different than the control groups. These measurements demonstrate that most cells tolerated the LbL nanocoating with aminated and carboxylated silks. Since the cell viability was not significantly affected by the 2 mg ml⁻¹ silk encapsulation process, this concentration was used for further experiments. We then quantified the cell viability of 2 mg ml⁻¹ silk encapsulation after each bilayer up to 5 bilayers.

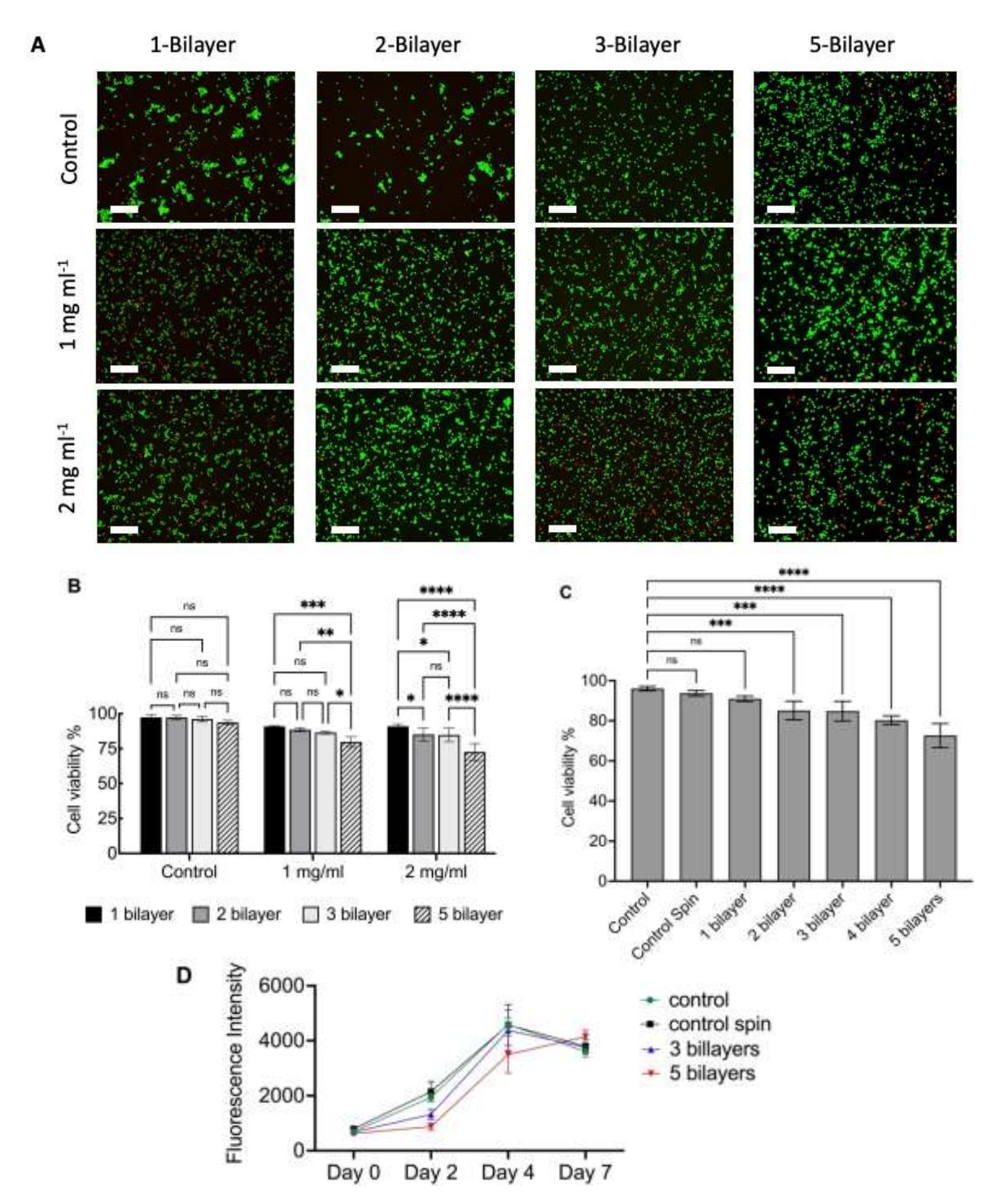


Figure 4. (A) Live/dead micrographs after different layers of silk coating at different concentrations. Scale bars: $500 \,\mu\text{m}$. (B) Quantification of cell viability for the control group postspin and experimental groups encapsulated with 1 mg/ml and 2 mg/ml silk concentrations after 3 and 5 bilayer applications (n = 5, *p < 0.05, **p < 0.01, ***p < 0.001 and ****p<0.0001) (C) Quantification of cell viability immediately following each bilayer application on day 0 (n = 5, *p < 0.05, **p < 0.01, ***p < 0.001 and ****p<0.0001) (D) Quantification of cell viability starting from day 0 to day 7 after encapsulation (2 mg/ml) using Alamar Blue cell viability kit.

The results showed 80% cell viability for up to 4 bilayers of encapsulation and around 72% for 5 bilayers. In addition to live/dead staining, we investigated the impact of silk encapsulation on overall cellular activities using an Alamar Blue assay from day 0 up to day 7 (Figure 4D). The results demonstrated that cellular metabolism and proliferation persisted in cells after the process of encapsulation, indicating that the silk coating did not adversely affect these vital cellular functions. Although the initial proliferation rate of cells encapsulated in silk coatings was lower on day 2 post-coating compared to uncoated cells, these cells continued to proliferate over time. By day 4, cells encapsulated in 3 bilayers reached activity levels comparable to non-coated cells. Similarly, cells with 5 bilayers achieved comparable activity levels by day 7 (Figure 4D). Alamar Blue readings for both the 3-bilayer and control groups began to decline slightly after day 4, likely due to cells in these groups reaching confluence and halting further proliferation, which in turn decreased their metabolic activity and led to reduced Alamar Blue readings. Meanwhile, cells in the 5-bilayer group, which started with a lower initial density, continued to proliferate. These observations suggest that the silk coating did not significantly impact long-term cell growth or cause significant cytotoxicity.

Next, we examined the persistence of the silk encapsulation on the surface of THP-1 cells. Encapsulated THP-1 cells with FITC-labeled aminated silk and carboxylated silk were incubated in growth media under standard culture conditions, and the cells were then observed using a fluorescence microscope over a period of 7 days. Across all the silk ionomer-coated groups with varying concentrations, a persistent green fluorescence signal was evident from the silk ionomer layers on THP-1 cells for up to three days in culture, with a gradual decline over time (Figure 5). By day 1, the silk layers surrounding some cells in the culture had disappeared,

and by day 3, this layer had dissipated in most cells. The fluorescence observed on day 3 predominantly originated from silk fragments in the culture media. Interestingly, the fluorescence signal from the cells encapsulated with 2 mg ml⁻¹ of silk had a higher intensity compared to the cells encapsulated with 1 mg ml⁻¹ on day 3 (Figure 5), showing a higher concentration contributed to more durable silk coatings. The detachment of silk coatings can be attributed to several factors. Silk fibroins, once deposited on the cell surface, remain there until the ongoing ion exchange processes and changes in membrane potential around metabolically active cells overcome the electrostatic interactions between the plasma membrane and the polyelectrolyte bilayers. Additionally, fluctuations in the pH of the culture due to metabolic activity can destabilize the charged bilayer. This instability may disrupt the ionic bridges between the layers, leading to the dissipation of the bilayers. Furthermore, the FITC signal detected within the cells after 24 hours indicates that a portion of the silk polyelectrolyte has been internalized by the cells, likely through the process of endocytosis. In our previous work, we demonstrated that the 3-bilayer silk ionomer coating on fibroblasts degraded over time, noticeable as early as day 1 post-coating - a beneficial characteristic for temporary cell encapsulation¹⁵. In this study, we applied the same 3-bilayer coating to THP-1 cells and observed similar degradation patterns to those seen with the fibroblasts. Given the potential for increased coating durability with greater thickness, we found it important to explore the persistence of a 5bilayer coating on THP-1 cells to determine if it extends the protective period without compromising cellular functionality. The ability of the silk ionomers to gradually dissociate from the cell surface indicated their potential as an effective coating material that can provide temporary cell protection without causing long-term interference with the cellular processes.

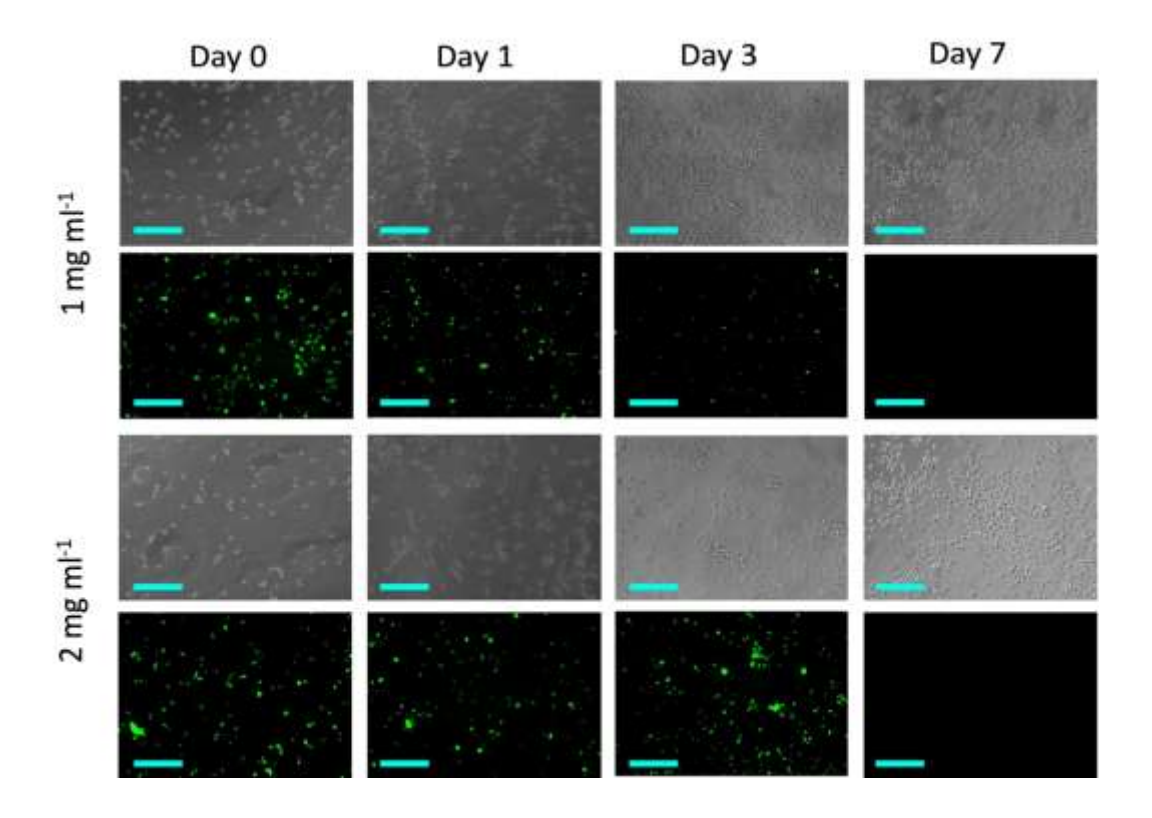


Figure 5. Fluorescence micrographs of the THP-1 cells encapsulated with 3 bilayer of FITC-labeled silk ionomers with different silk concentrations from day 0 to day 7. Scale bar: $150 \mu m$.

3.4 Atomic Force Microscopy (AFM) Measurements of stiffness of encapsulated cells

The impact of silk encapsulation on the stiffness of cellular surfaces was assessed by AFM. Specifically, we were interested in determining if an increase in surface stiffness was observed post-encapsulation and whether this change correlated with the number of coating layers. AFM indentation measurements was utilized to obtain elasticity maps of non-coated THP-1 cells, as well as cells with 3 and 5 bilayers of silk coating. A mathematical model was also used to predict the elastic modulus for a composite layer/substrate system.

The topography of a single cell imaged using the contact mode of the AFM is shown in Figure 6A, while Figures 6B and C display a sample AFM-acquired height profile and elasticity map, respectively, for the same cell. The cell height image (Figure 6B) revealed the cell boundary and topography through the clear color contrast between the cell (in blue) and the substrate (in red). The elasticity map (Figure 6C) illustrates the distribution of elastic modulus across the cell surface. The elastic moduli are obtained by averaging the measured values at each point on the map. Figure 6C indicates that there was no significant variation in the elastic modulus across the cell surface, with values ranging from 100 kPa to 150 kPa.

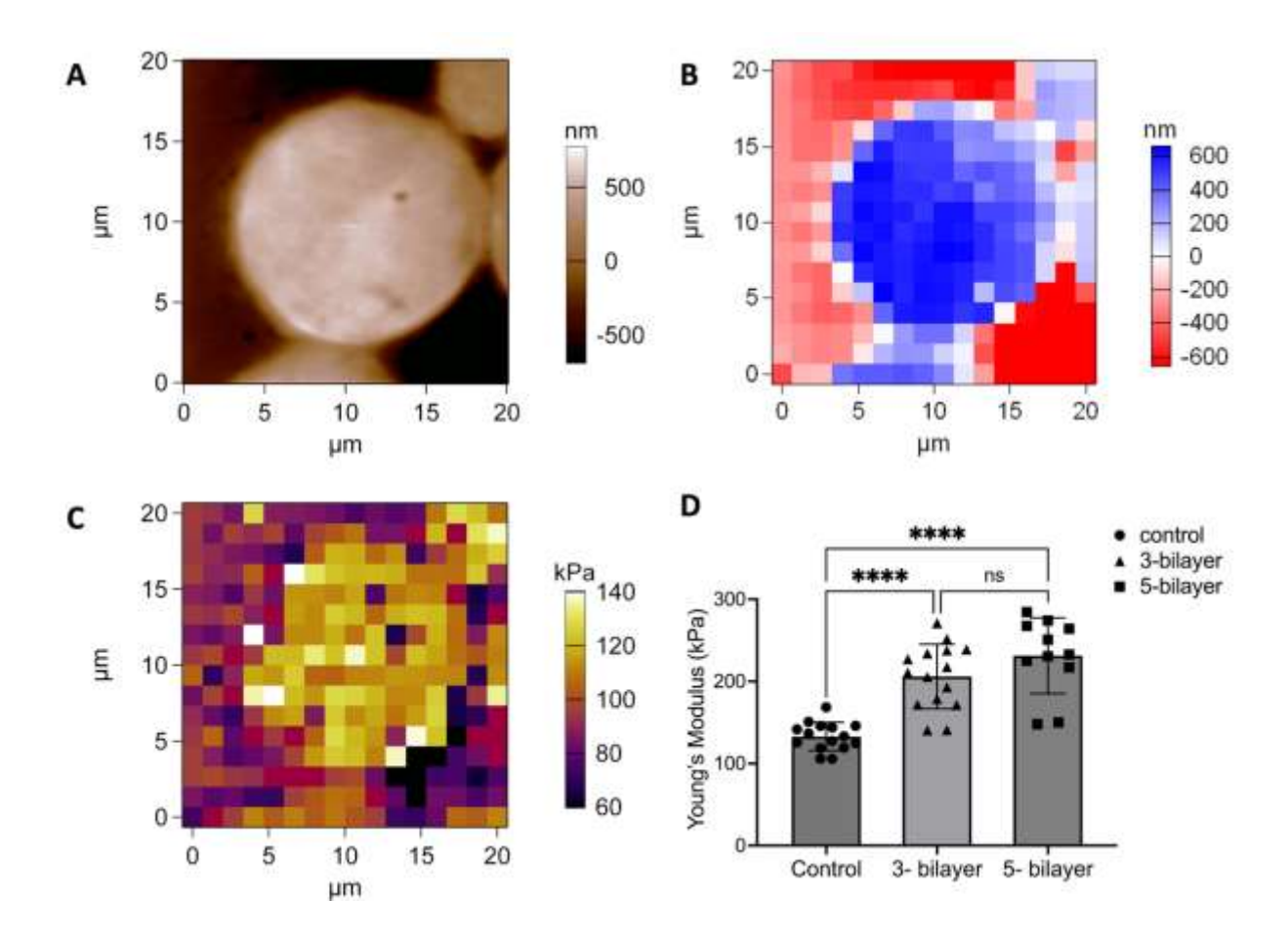


Figure 6. (A) the topography of a sample of a single cell imaged using the contact mode of the AFM; (B) height distribution for the cell shown in (A), and (C) elasticity map acquired for the same cell shown in (B); (D) graph representing measured stiffness using AFM for control, 3-bilayer and 5-bilayer experimental groups of encapsulations. (n = 5, p < 0.05, **p < 0.01, and ****p < 0.0001)

These results show a significant difference in the mechanical properties of THP-1 cells before and after encapsulation. The measured average elastic modulus of noncoated THP-1 was 132.90 ± 17.21 kPa. In contrast, cells encapsulated with 3 and 5 bilayers of silk exhibited significantly increased stiffness compared to the control group, with average elastic moduli of 206.11 ± 39.29 kPa and 231.35 ± 46.10 kPa, respectively (Figure 6D). The AFM force–

indentation experiments show that the increase in stiffness of encapsulated cells with silk bilayers is statistically significant compared to the uncoated cells.

Furthermore, we used an elastic model based on the modified Bec/Tonck model to predict how the thickness of the silk bilayer affected the stiffness of the encapsulated cell. The Bec/Tonck model has been previously used to calculate stiffness variations with coated layer thickness in different coating systems ⁵⁸⁻⁶⁰. This model has been refined into a two-layer model as given in eq. (01) by Pailler-Mattei et al.⁵³ and used to predict the stiffness considering two thin layers on a substrate.

$$E^* = E_1 E_2 E_S \frac{\pi^2 a^2 + \pi a (4e_1 + 2e_2) + 2e_1 (2e_1 + 2e_2)}{\pi^2 a^2 E_1 E_2 + 2\pi a (e_1 E_S E_2 + e_2 E_S E_2 + e_1 E_1 E_2) + 2e_1 E_S E_2 (2e_1 + 2e_2)}$$
eq.01

In eq. 01, E^* is the global elastic modulus of the cell-silk system, which can be measured using AFM indentation, while a is the contact radius of the projected contact area during indentation. The parameters e_1 and e_2 are the thickness of the two layers. E_1 , E_2 , and E_S are the elastic moduli of the two layers and substrates, respectively⁵³.

In this paper, we simplify the model given by eq. 01 by considering one bilayer as a single coating layer as shown in Figure 7A. Hence, the model parameters become $E_1=E_2=E$ and $e_1=e_2=e$, where E is the elastic modulus and e is the thickness of the bilayer, and eq. 01 reduces to:

$$E^* = EE_S \frac{\pi a^2 + 6\pi a e + 8e^2}{\pi^2 a^2 E + 2\pi a e (2E_S + E) + 8e^2 E_S}$$
eq.02

Eq. 02 satisfies the conditions that $E^* \to E_s$ as $e \to 0$ where the global stiffness becomes the substrate stiffness and $E^* \to E$ as $e \to \infty$ where the effect from the substrate is negligible due to the significant thickness of the bilayer.

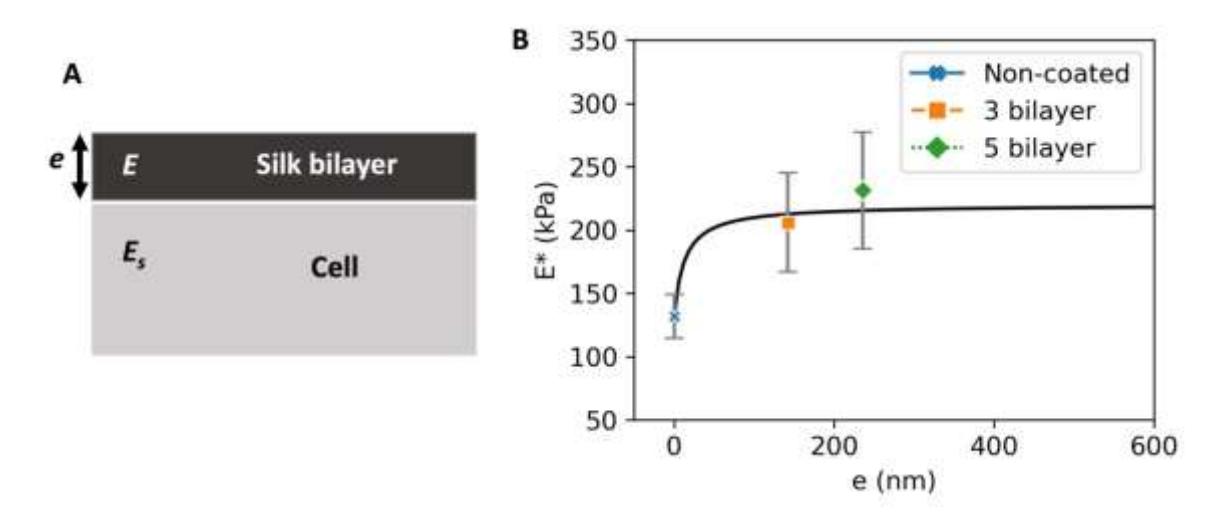


Figure 7. (A) Schematic diagram showing a single layer on a substrate, used as a model for silk-coated cells. 'E' represents the elastic modulus of the silk bilayer, while 'Es' represents the modulus of the cell. 'e' indicates the thickness of the silk bilayer. (B) Graph depicting the variation of the effective modulus (E*) as a function of 'e', according to the model (illustrated by the black curve). The stiffness of non-coated cells is indicated by a blue point at e=0. The orange and green points represent the measured stiffness of cells encapsulated with 3-bilayers and 5-bilayers, respectively.

We calculated the elastic modulus of the silk-coated cell system using eq. 02 using the following parameters: a) $E_s = 132.90$ kPa, the substrate stiffness = stiffness of the cell, which is measured from non-coated cells using AFM; b) E=220 kPa the stiffness of a single silk bilayer; and c) the thickness of 3 bilayers and 5 bilayers: e=142 nm and 236 nm, respectively. The thickness of the silk bilayers was calculated using QCM-D analysis¹⁵.

For the stiffness of the bilayer we used the values reported in our previous work¹⁵. The calculated elastic modulus for 3 bilayers and 5 bilayers of encapsulated cells using the model were 212.57 kPa and 215.37 kPa, respectively; both of these values are within the standard deviation of the measured value as shown in error bars of red and the green point on the plot of Figure 7B. Additionally, we use eq. 02 to plot the variation of elastic modulus E^* as a function or thickness e, and thus to predict the values of the elastic modulus for the composed system for unknown values of the thickness parameter e (Figure 7B). The black curve in Figure 7B shows that the elastic modulus reaches a constant value above a specific threshold thickness $e \approx 150$ nm, thus predicting that increasing the number of bilayers above this threshold will not significantly affect the overall stiffness of the system.

4. DISCUSSION

The results presented in this study demonstrate the successful encapsulation of THP-1 cells using silk-ionomer deposition, which can provide temporary cell protection without causing interference with regular cellular processes. The THP-1 cell line is isolated from the peripheral blood of a patient with acute monocytic leukemia, which has the ability to differentiate into macrophages. This cell line has been widely used in studying immune responses, signaling pathways, and nutrient and drug transport while cells are in the monocyte state as well as in the macrophage state⁶¹. Encapsulation of immune cells, such as THP-1 cells, has often been done in immunotherapy and related experimental applications⁴³⁻⁴⁶. Such cellular encapsulation can shield immune cells from the host's immune response, which can reduce the risk of rejection and improve the longevity of the transplanted cells particularly in cases where the immune cells are modified or engineered for therapeutic purposes. Additionally, encapsulation can provide a controlled environment that can help to maintain the function and phenotype of the encapsulated

immune cells. In cell-based therapies, encapsulated immune cells can be transplanted into the body to modulate the immune response ⁶². For example, encapsulated antigen-presenting cells can be used to stimulate the immune response in cancer immunotherapy ⁶³.

The materials used for encapsulation must be biocompatible and must allow the exchange of oxygen, nutrients, and metabolites while concealing the encapsulated cells from the host's immune system. Many types of natural and synthetic materials are being explored with different methods and techniques of encapsulation⁶⁴⁻⁶⁸. Among these materials, silk is a useful biomaterial with biocompatibility, ease of chemical modification, gradual in vivo degradation, and potential to be changed into different biomaterial formats either in aqueous solution or organic solvent⁶⁹. Silk fibroin is a protein block copolymer consisting of hydrophobic β-sheet-forming domains linked through hydrophilic domains. These arrangements give rise to a resilient protein with high tensile strength and toughness in fiber form. The tensile strength of silk fibroin fibers (740 MPa) provides improved strength than the commonly used degradable polymeric biomaterials, especially collagen (0.9–7.4 MPa) and poly(L-lactic acid) (PLA) (28–50 MPa)^{29, 70}.

With these beneficial properties, silk-based materials used to encapsulate THP-1 cells can create a protective microenvironment for the cells. This method holds promise as a tool for studying immune cell biology and developing potential immunotherapeutic strategies, while maintaining normal cellular processes. For example, encapsulation using silk fibroin with polylysine hydrobromide (PL) and poly-glutamic (PG) acid sodium salts layers on living yeast cells or the bacterial strains *E. coli* and *B. subtilis* were previously reported ^{20, 37-38}. These materials showed cytotoxicity to mammalian cells, depending on charge density, molecular weight, or concentration of polycations^{15, 71}. To minimize cytotoxicity towards the mammalian cells a novel method of synthesis of silk ionomers was developed involving the carboxylation and amination

of SF with a lower charge density and used to successfully coat murine fibroblasts (L929) and human mesenchymal stem cells (hMSCs) with retention of cell viability of above 90% and 80%, respectively¹⁵. Similar results were shown in our present study, where we used the carboxylate and aminated SF ionomers to encapsulate THP-1 cells using electrostatic layer-by-layer deposition and 80% of the encapsulated cells were viable after 3 bilayers of encapsulation (Figure 4C). THP-1 cells were encapsulated with up to 5 bilayers, with 80% cell viability for up to 4 bilayers of encapsulation and around 72% for 5 bilayers (Figure 4C). The Alamar Blue assay results indicate that cellular metabolism and proliferation remain unaffected in THP-1 cells following encapsulation, suggesting that the silk coating preserves vital cellular functions. The biodegradable nature of silk ionomers ⁷²⁻⁷³, which allows them to disintegrate over time, is advantageous for generating a temporary protective barrier that does not permanently interfere with cellular activities. In this study, the fluorescence microscopy observations of encapsulated THP-1 cells with FITC-labeled silk ionomers showcased green fluorescence, suggesting the presence of silk ionomer layers for up to three days in culture. Notably, this fluorescence signal weakens and vanishes entirely by the seventh day, illustrating silk ionomer degradation. This progressive decline in signal intensity implies the silk ionomers are breaking down over time, a desirable characteristic for temporary cell protection coatings⁷⁴. Our experiments demonstrated that cells encapsulated with 3 bilayers maintain approximately 80% viability (Figure 4C), supporting cell integrity and functionality. This encapsulation also enhances the mechanical stiffness of the cells. On the other hand, increasing the encapsulation to 5 bilayers boosts the mechanical stiffness further, which enhances the cells' protection and increases their resistance to external stresses. However, this increase comes with a reduction in cell viability, which drops to about 72% (Figure 4C). While 3 bilayers offer effective protection and maintain higher cell

viability along with good mechanical stability, 5 bilayers provide superior protection and mechanical strength at the expense of lower cell viability. The decrease in cell viability with 5 bilayers suggests a trade-off that may not be suitable for all applications. Thus, the choice between 3 and 5 bilayers should be guided by specific application needs, balancing optimal protection, cell viability, and mechanical properties. The tunability of the coating layers highlights the adaptability of our approach to different operational requirements.

The characterization of surface morphology and mechanical properties of encapsulated cells provides insight into the effectiveness of the encapsulation technique ⁷⁵. In this paper, we utilized SEM, confocal microscopy, and AFM to examine the outcomes of encapsulation. SEM images of encapsulated cells showed a uniform coating around cells, confirming successful encapsulation. This observation was further supported by confocal microscopy, which illustrated complete encapsulation. Furthermore, AFM analysis revealed an increase in the stiffness of the encapsulated cells. We used the modified Bec/Tonck model to predict the variation of the elastic modulus of the encapsulated cells with the thickness of the silk bilayers. We found that the elastic modulus stabilized at a constant value once the thickness exceeded a threshold (e ≈ 150 nm). This suggests that adding more bilayers beyond this point will not significantly influence the overall stiffness. Based on the AFM and cell viability results, we conclude that increasing the number of bilayers beyond 5 likely will not contribute to an increase in stiffness while also decreasing cell viability. The application of this mathematical model introduces a novel approach to existing research by predicting the outcome of the stiffness. By integrating this model, we have achieved a better understanding of the broader applicability and limitations of cell encapsulation. This approach has the potential to provide valuable insights into the encapsulation of new types of cells.

In future work, we will investigate the functionality of THP-1 cells post-encapsulation by

specifically testing their ability to differentiate into macrophages. We also plan to evaluate the

cytoprotective effects of the encapsulation barrier using specific immunostained surface markers.

Furthermore, we will explore the preservation of cell viability and growth against hydrodynamic

forces during extrusion-based delivery.

5. CONCLUSIONS

We demonstrated the successful encapsulation of THP-1 immune cells using silk-ionomer

deposition, highlighting the preservation of cell viability and proliferation. We demonstrated that

silk-ionomer coatings did not adversely affect cellular metabolism and proliferation and thus

have the potential for bioengineering applications or processes that require temporary cell

protection. The ability of silk ionomers to degrade over time further supports their suitability for

creating a protective barrier without long-term interference with cellular processes. We have also

shown that the stiffness of the cells can be increased by encapsulating them in silk biomaterials,

and that the call-biomaterial stiffness can be tuned by changing the number of bilayers used for

encapsulation. Moreover, we have established a correlation between the stiffness of encapsulated

cells and the thickness of the silk bilayer, employing a modified Bec/Tonck model. We have

used this model to predict the stiffness of the encapsulated cells. Our findings underscore the

promising role of silk-ionomer encapsulation for immune cells.

AUTHOR INFORMATION

Corresponding Author

Ying Chen- Department of Biomedical Engineering, Tufts University, Medford, MA

Email: ying.chen@tufts.edu

28

David L. Kaplan- Department of Biomedical Engineering, Tufts University, Medford, MA

Email: david.kaplan@tufts.edu

Cristian Staii- Department of Physics and Astronomy, Tufts University, Medford, MA

Email: cristian.staii@tufts.edu

Author Contributions

The manuscript was written through the contributions of all authors. All authors have given

approval to the final version of the manuscript.

Acknowledgments

The SEM imaging in this work was performed in part at the Harvard University Center for

Nanoscale Systems (CNS), a member of the National Nanotechnology Coordinated

Infrastructure Network (NNCI).

Funding Statement

We thank the National Science Foundation (DMR2104294) for the support of this work.

Abbreviations

LbL, Layer by layer; SF, Silk fibroin; AFM, Atomic Force Microscope: SEM, Scanning Electron

Microscope

Supporting Information: Figure S1

29

REFERENCES

- 1. Li, W.; Lei, X.; Feng, H.; Li, B.; Kong, J.; Xing, M., Layer-by-Layer Cell Encapsulation for Drug Delivery: The History, Technique Basis, and Applications. *Pharmaceutics* **2022**, *14* (2). DOI: 10.3390/pharmaceutics14020297.
- 2. Guerzoni, L. P. B.; Tsukamoto, Y.; Gehlen, D. B.; Rommel, D.; Haraszti, T.; Akashi, M.; De Laporte, L., A Layer-by-Layer Single-Cell Coating Technique To Produce Injectable Beating Mini Heart Tissues via Microfluidics. *Biomacromolecules* **2019**, *20* (10), 3746-3754. DOI: 10.1021/acs.biomac.9b00786.
- 3. Hasturk, O.; Kaplan, D. L., Cell armor for protection against environmental stress: Advances, challenges and applications in micro- and nanoencapsulation of mammalian cells. *Acta Biomater* **2019**, *95*, 3-31. DOI: 10.1016/j.actbio.2018.11.040.
- 4. Granicka, L. H., Nanoencapsulation of cells within multilayer shells for biomedical applications. *J Nanosci Nanotechnol* **2014**, *14* (1), 705-16. DOI: 10.1166/jnn.2014.9106.
- 5. Lee, J.; Choi, J.; Park, J. H.; Kim, M.-H.; Hong, D.; Cho, H.; Yang, S. H.; Choi, I. S., Cytoprotective Silica Coating of Individual Mammalian Cells through Bioinspired Silicification. *Angewandte Chemie International Edition* **2014**, *53* (31), 8056-8059. DOI: https://doi.org/10.1002/anie.201402280.
- 6. Lee, H.; Kim, N.; Rheem, H. B.; Kim, B. J.; Park, J. H.; Choi, I. S., A Decade of Advances in Single-Cell Nanocoating for Mammalian Cells. *Advanced Healthcare Materials* **2021**, *10* (13), 2100347. DOI: https://doi.org/10.1002/adhm.202100347.
- 7. Batorsky, A.; Liao, J.; Lund, A. W.; Plopper, G. E.; Stegemann, J. P., Encapsulation of adult human mesenchymal stem cells within collagen-agarose microenvironments. *Biotechnol Bioeng* **2005**, *92* (4), 492-500. DOI: 10.1002/bit.20614.
- 8. Karoubi, G.; Ormiston, M. L.; Stewart, D. J.; Courtman, D. W., Single-cell hydrogel encapsulation for enhanced survival of human marrow stromal cells. *Biomaterials* **2009**, *30* (29), 5445-55. DOI: 10.1016/j.biomaterials.2009.06.035.
- 9. Cooper, S. T.; McNeil, P. L., Membrane Repair: Mechanisms and Pathophysiology. *Physiol Rev* **2015**, *95* (4), 1205-40. DOI: 10.1152/physrev.00037.2014.

- 10. McNeil, P. L.; Steinhardt, R. A., Plasma membrane disruption: repair, prevention, adaptation. *Annu Rev Cell Dev Biol* **2003**, *19*, 697-731. DOI: 10.1146/annurev.cellbio.19.111301.140101.
- 11. Cui, X.; Dean, D.; Ruggeri, Z. M.; Boland, T., Cell damage evaluation of thermal inkjet printed Chinese hamster ovary cells. *Biotechnol Bioeng* **2010**, *106* (6), 963-9. DOI: 10.1002/bit.22762.
- 12. Hasturk, O.; Rodriguez, M. J.; Wheeler, J. J.; Venoor, V.; Sobkowicz, M. J.; Kaplan, D. L., Silk nanocoatings of mammalian cells for cytoprotection against mechanical stress. *MRS Bulletin* **2021**, *46* (9), 795-806. DOI: 10.1557/s43577-021-00114-3.
- 13. Yang, J.; Li, J.; Li, X.; Wang, X.; Yang, Y.; Kawazoe, N.; Chen, G., Nanoencapsulation of individual mammalian cells with cytoprotective polymer shell. *Biomaterials* **2017**, *133*, 253-262. DOI: https://doi.org/10.1016/j.biomaterials.2017.04.020.
- 14. Yang, S. H.; Kang, S. M.; Lee, K.-B.; Chung, T. D.; Lee, H.; Choi, I. S., Mussel-Inspired Encapsulation and Functionalization of Individual Yeast Cells. *Journal of the American Chemical Society* **2011**, *133* (9), 2795-2797. DOI: 10.1021/ja1100189.
- 15. Hasturk, O.; Sahoo, J. K.; Kaplan, D. L., Synthesis and Characterization of Silk Ionomers for Layer-by-Layer Electrostatic Deposition on Individual Mammalian Cells. *Biomacromolecules* **2020**, *21* (7), 2829-2843. DOI: 10.1021/acs.biomac.0c00523.
- 16. Li, W.; Zhang, G.; Guan, T.; Zhang, X.; Khosrozadeh, A.; Xing, M.; Kong, J., Manipulable Permeability of Nanogel Encapsulation on Cells Exerts Protective Effect against TNF-α-Induced Apoptosis. *ACS Biomater Sci Eng* **2018**, *4* (8), 2825-2835. DOI: 10.1021/acsbiomaterials.8b00654.
- 17. Liu, D.; Nikoo, M.; Boran, G.; Zhou, P.; Regenstein, J. M., Collagen and gelatin. *Annu Rev Food Sci Technol* **2015**, *6*, 527-57. DOI: 10.1146/annurev-food-031414-111800.
- 18. Velasco-Mallorquí, F.; Rodríguez-Comas, J.; Ramón-Azcón, J., Cellulose-based scaffolds enhance pseudoislets formation and functionality. *Biofabrication* **2021**, *13* (3). DOI: 10.1088/1758-5090/ac00c3.
- 19. Gattás-Asfura, K. M.; Stabler, C. L., Bioorthogonal layer-by-layer encapsulation of pancreatic islets via hyperbranched polymers. *ACS Appl Mater Interfaces* **2013**, *5* (20), 9964-74. DOI: 10.1021/am401981g.

- 20. Veerabadran, N. G.; Goli, P. L.; Stewart-Clark, S. S.; Lvov, Y. M.; Mills, D. K., Nanoencapsulation of Stem Cells within Polyelectrolyte Multilayer Shells. *Macromolecular Bioscience* **2007**, *7* (7), 877-882. DOI: https://doi.org/10.1002/mabi.200700061.
- 21. Kim, M.; Erickson, I. E.; Huang, A. H.; Garrity, S. T.; Mauck, R. L.; Steinberg, D. R., Donor Variation and Optimization of Human Mesenchymal Stem Cell Chondrogenesis in Hyaluronic Acid. *Tissue Eng Part A* **2018**, *24* (21-22), 1693-1703. DOI: 10.1089/ten.TEA.2017.0520.
- 22. Genç, H.; Hazur, J.; Karakaya, E.; Dietel, B.; Bider, F.; Groll, J.; Alexiou, C.; Boccaccini, A. R.; Detsch, R.; Cicha, I., Differential Responses to Bioink-Induced Oxidative Stress in Endothelial Cells and Fibroblasts. *Int J Mol Sci* **2021**, *22* (5). DOI: 10.3390/ijms22052358.
- 23. Matsuzawa, A.; Matsusaki, M.; Akashi, M., Effectiveness of Nanometer-Sized Extracellular Matrix Layer-by-Layer Assembled Films for a Cell Membrane Coating Protecting Cells from Physical Stress. *Langmuir* **2013**, *29* (24), 7362-7368. DOI: 10.1021/la303459v.
- 24. Murakami, Y.; Iwata, H.; Kitano, E.; Kitamura, H.; Ikada, Y., Interaction of poly(styrene sulfonic acid) with the classical pathway of the serum complement system. *J Biomater Sci Polym Ed* **2005**, *16* (6), 685-97. DOI: 10.1163/1568562053992469.
- 25. Åkerfeldt, M.; Nilsson, E.; Gillgard, P.; Walkenström, P., Textile piezoelectric sensors melt spun bi-component poly(vinylidene fluoride) fibres with conductive cores and poly(3,4-ethylene dioxythiophene)-poly(styrene sulfonate) coating as the outer electrode. *Fashion and Textiles* **2014**, *I* (1), 13. DOI: 10.1186/s40691-014-0013-6.
- 26. Vepari, C.; Kaplan, D. L., Silk as a Biomaterial. *Prog Polym Sci* **2007**, *32* (8-9), 991-1007. DOI: 10.1016/j.progpolymsci.2007.05.013.
- 27. Xiao, L.; Liu, S.; Yao, D.; Ding, Z.; Fan, Z.; Lu, Q.; Kaplan, D. L., Fabrication of Silk Scaffolds with Nanomicroscaled Structures and Tunable Stiffness. *Biomacromolecules* **2017**, *18* (7), 2073-2079. DOI: 10.1021/acs.biomac.7b00406.
- 28. Bono, N.; Saroglia, G.; Marcuzzo, S.; Giagnorio, E.; Lauria, G.; Rosini, E.; De Nardo, L.; Athanassiou, A.; Candiani, G.; Perotto, G., Silk fibroin microgels as a platform for cell microencapsulation. *J Mater Sci Mater Med* **2022**, *34* (1), 3. DOI: 10.1007/s10856-022-06706-y.

- 29. Wang, X.; Kluge, J. A.; Leisk, G. G.; Kaplan, D. L., Sonication-induced gelation of silk fibroin for cell encapsulation. *Biomaterials* **2008**, *29* (8), 1054-64. DOI: 10.1016/j.biomaterials.2007.11.003.
- 30. Johari, N.; Moroni, L.; Samadikuchaksaraei, A., Tuning the conformation and mechanical properties of silk fibroin hydrogels. *European Polymer Journal* **2020**, *134*, 109842. DOI: https://doi.org/10.1016/j.eurpolymj.2020.109842.
- 31. Silva, S. S.; Motta, A.; Rodrigues, M. T.; Pinheiro, A. F. M.; Gomes, M. E.; Mano, J. F.; Reis, R. L.; Migliaresi, C., Novel Genipin-Cross-Linked Chitosan/Silk Fibroin Sponges for Cartilage Engineering Strategies. *Biomacromolecules* **2008**, *9* (10), 2764-2774. DOI: 10.1021/bm800874q.
- 32. Taddei, P.; Chiono, V.; Anghileri, A.; Vozzi, G.; Freddi, G.; Ciardelli, G., Silk Fibroin/Gelatin Blend Films Crosslinked with Enzymes for Biomedical Applications. *Macromolecular Bioscience* **2013**, *13* (11), 1492-1510. DOI: https://doi.org/10.1002/mabi.201300156.
- 33. Wang, X.; Zhao, P.; Li, Y.; Yi, Q.; Ma, S.; Xie, K.; Chen, H.; Xia, Q., Modifying the Mechanical Properties of Silk Fiber by Genetically Disrupting the Ionic Environment for Silk Formation. *Biomacromolecules* **2015**, *16* (10), 3119-3125. DOI: 10.1021/acs.biomac.5b00724.
- 34. Murphy, A. R.; Kaplan, D. L., Biomedical applications of chemically-modified silk fibroin. *Journal of Materials Chemistry* **2009**, *19* (36), 6443-6450. DOI: 10.1039/B905802H.
- 35. Gouaux, E.; Mackinnon, R., Principles of selective ion transport in channels and pumps. *Science* **2005**, *310* (5753), 1461-5. DOI: 10.1126/science.1113666.
- 36. Adams, D. S.; Levin, M., General principles for measuring resting membrane potential and ion concentration using fluorescent bioelectricity reporters. *Cold Spring Harb Protoc* **2012**, *2012* (4), 385-97. DOI: 10.1101/pdb.top067710.
- 37. Drachuk, I.; Calabrese, R.; Harbaugh, S.; Kelley-Loughnane, N.; Kaplan, D. L.; Stone, M.; Tsukruk, V. V., Silk macromolecules with amino acid-poly(ethylene glycol) grafts for controlling layer-by-layer encapsulation and aggregation of recombinant bacterial cells. *ACS Nano* **2015**, *9* (2), 1219-35. DOI: 10.1021/nn504890z.
- 38. Serban, M. A.; Kaplan, D. L., pH-Sensitive ionomeric particles obtained via chemical conjugation of silk with poly(amino acid)s. *Biomacromolecules* **2010**, *11* (12), 3406-12. DOI: 10.1021/bm100925s.

- 39. Murphy, A. R.; St John, P.; Kaplan, D. L., Modification of silk fibroin using diazonium coupling chemistry and the effects on hMSC proliferation and differentiation. *Biomaterials* **2008**, 29 (19), 2829-38. DOI: 10.1016/j.biomaterials.2008.03.039.
- 40. Chanput, W.; Mes, J. J.; Wichers, H. J., THP-1 cell line: An in vitro cell model for immune modulation approach. *International Immunopharmacology* **2014**, *23* (1), 37-45. DOI: https://doi.org/10.1016/j.intimp.2014.08.002.
- 41. Qin, Z., The use of THP-1 cells as a model for mimicking the function and regulation of monocytes and macrophages in the vasculature. *Atherosclerosis* **2012**, *221* (1), 2-11. DOI: https://doi.org/10.1016/j.atherosclerosis.2011.09.003.
- 42. Chanput, W.; Peters, V.; Wichers, H., THP-1 and U937 Cells. In *The Impact of Food Bioactives on Health: in vitro and ex vivo models*, Verhoeckx, K.; Cotter, P.; López-Expósito, I.; Kleiveland, C.; Lea, T.; Mackie, A.; Requena, T.; Swiatecka, D.; Wichers, H., Eds. Springer International Publishing: Cham, 2015; pp 147-159. DOI: 10.1007/978-3-319-16104-4 14.
- 43. Wattanakull, P.; Killingsworth, M. C.; Pissuwan, D., Biological responses of T cells encapsulated with polyelectrolyte-coated gold nanorods and their cellular activities in a co-culture system. *Applied Nanoscience* **2017**, *7* (8), 667-679. DOI: 10.1007/s13204-017-0605-8.
- 44. Borkowska, M.; Grzeczkowicz, A.; Strawski, M.; Kawiak, J.; Szklarczyk, M.; Granicka, L. H., Performance and detection of nano-thin polyelectrolyte shell for cell coating. *Journal of Nanoparticle Research* **2014**, *16* (7), 2488. DOI: 10.1007/s11051-014-2488-x.
- 45. Zhang, Q.; Dehaini, D.; Zhang, Y.; Zhou, J.; Chen, X.; Zhang, L.; Fang, R. H.; Gao, W.; Zhang, L., Neutrophil membrane-coated nanoparticles inhibit synovial inflammation and alleviate joint damage in inflammatory arthritis. *Nat Nanotechnol* **2018**, *13* (12), 1182-1190. DOI: 10.1038/s41565-018-0254-4.
- 46. Ščigalková, I.; Bystroňová, J.; Kovářová, L.; Pravda, M.; Velebný, V.; Riabov, V.; Klüter, H.; Kzhyshkowska, J.; Vrana, N. E., The effect of healing phenotype-inducing cytokine formulations within soft hydrogels on encapsulated monocytes and incoming immune cells. *RSC Advances* **2019**, *9* (37), 21396-21404. DOI: 10.1039/C9RA02878A.
- 47. Solon, J.; Levental, I.; Sengupta, K.; Georges, P. C.; Janmey, P. A., Fibroblast adaptation and stiffness matching to soft elastic substrates. *Biophys J* **2007**, *93* (12), 4453-61. DOI: 10.1529/biophysj.106.101386.

- 48. Wu, H. W.; Kuhn, T.; Moy, V. T., Mechanical properties of L929 cells measured by atomic force microscopy: effects of anticytoskeletal drugs and membrane crosslinking. *Scanning* **1998**, *20* (5), 389-97. DOI: 10.1002/sca.1998.4950200504.
- 49. Radmacher, M.; Fritz, M.; Kacher, C. M.; Cleveland, J. P.; Hansma, P. K., Measuring the viscoelastic properties of human platelets with the atomic force microscope. *Biophys J* **1996**, *70* (1), 556-67. DOI: 10.1016/s0006-3495(96)79602-9.
- 50. Liu, F.; Tschumperlin, D. J., Micro-mechanical characterization of lung tissue using atomic force microscopy. *J Vis Exp* **2011**, (54). DOI: 10.3791/2911.
- 51. Sunnerberg, J. P.; Moore, P.; Spedden, E.; Kaplan, D. L.; Staii, C., Variations of Elastic Modulus and Cell Volume with Temperature for Cortical Neurons. *Langmuir* **2019**, *35* (33), 10965-10976. DOI: 10.1021/acs.langmuir.9b01651.
- 52. Kumarasinghe, U.; Fox, L. N.; Staii, C., Combined Traction Force– Atomic Force Microscopy Measurements of Neuronal Cells. *Biomimetics* **2022**, *7* (4), 157.
- 53. Pailler-Mattei, C.; Bec, S.; Zahouani, H., In vivo measurements of the elastic mechanical properties of human skin by indentation tests. *Medical Engineering & Physics* **2008**, *30* (5), 599-606. DOI: https://doi.org/10.1016/j.medengphy.2007.06.011.
- 54. Chen, Y.; Williams, A. M.; Gordon, E. B.; Rudolph, S. E.; Longo, B. N.; Li, G.; Kaplan, D. L., Biological effects of polystyrene micro- and nano-plastics on human intestinal organoid-derived epithelial tissue models without and with M cells. *Nanomedicine* **2023**, *50*, 102680. DOI: 10.1016/j.nano.2023.102680.
- 55. Chen, Y.; Rudolph, S. E.; Longo, B. N.; Pace, F.; Roh, T. T.; Condruti, R.; Gee, M.; Watnick, P. I.; Kaplan, D. L., Bioengineered 3D Tissue Model of Intestine Epithelium with Oxygen Gradients to Sustain Human Gut Microbiome. *Adv Healthc Mater* **2022**, *11* (16), e2200447. DOI: 10.1002/adhm.202200447.
- 56. Yu, C.; Zhao, W.; Duan, C.; Xie, J.; Yin, W., Poly-l-lysine-caused cell adhesion induces pyroptosis in THP-1 monocytes. *Open Life Sciences* **2022**, *17* (1), 279-283. DOI: doi:10.1515/biol-2022-0028.
- 57. Deleon, H.; Kuang, A.; Rugama, F. C.; Eubanks, T. M. In *Modified SEM Preparation for THP-1 Monocytes*, 2017.

- 58. Menga, N.; Putignano, C.; Afferrante, L.; Carbone, G., The Contact Mechanics of Coated Elastic Solids: Effect of Coating Thickness and Stiffness. *Tribology Letters* **2019**, *67* (1), 24. DOI: 10.1007/s11249-019-1137-z.
- 59. Bec, S.; Tonck, A.; Loubet, J. L., A simple guide to determine elastic properties of films on substrate from nanoindentation experiments. *Philosophical Magazine* **2006**, *86* (33-35), 5347-5358. DOI: 10.1080/14786430600660856.
- 60. Berla, L. A.; Aileen, A. M.; Han Min, S.; Nix, W. D., A physically based model for indenter tip shape calibration for nanoindentation. *Journal of Materials Research* **2010**, *25* (4), 735-745. DOI: 10.1557/JMR.2010.0098.
- 61. Daigneault, M.; Preston, J. A.; Marriott, H. M.; Whyte, M. K. B.; Dockrell, D. H., The Identification of Markers of Macrophage Differentiation in PMA-Stimulated THP-1 Cells and Monocyte-Derived Macrophages. *PLOS ONE* **2010**, *5* (1), e8668. DOI: 10.1371/journal.pone.0008668.
- 62. Wang, H.; Mooney, D. J., Biomaterial-assisted targeted modulation of immune cells in cancer treatment. *Nat Mater* **2018**, *17* (9), 761-772. DOI: 10.1038/s41563-018-0147-9.
- 63. Scheffel, F.; Knuschke, T.; Otto, L.; Kollenda, S.; Sokolova, V.; Cosmovici, C.; Buer, J.; Timm, J.; Epple, M.; Westendorf, A. M., Effective Activation of Human Antigen-Presenting Cells and Cytotoxic CD8(+) T Cells by a Calcium Phosphate-Based Nanoparticle Vaccine Delivery System. *Vaccines (Basel)* **2020**, *8* (1). DOI: 10.3390/vaccines8010110.
- 64. Weber, L. M.; He, J.; Bradley, B.; Haskins, K.; Anseth, K. S., PEG-based hydrogels as an in vitro encapsulation platform for testing controlled beta-cell microenvironments. *Acta Biomater* **2006**, *2* (1), 1-8. DOI: 10.1016/j.actbio.2005.10.005.
- 65. Stahl, P. J.; Romano, N. H.; Wirtz, D.; Yu, S. M., PEG-based hydrogels with collagen mimetic peptide-mediated and tunable physical cross-links. *Biomacromolecules* **2010**, *11* (9), 2336-44. DOI: 10.1021/bm100465q.
- 66. Hoshikawa, A.; Nakayama, Y.; Matsuda, T.; Oda, H.; Nakamura, K.; Mabuchi, K., Encapsulation of chondrocytes in photopolymerizable styrenated gelatin for cartilage tissue engineering. *Tissue Eng* **2006**, *12* (8), 2333-41. DOI: 10.1089/ten.2006.12.2333.
- 67. Fakhari, A.; Berkland, C., Applications and emerging trends of hyaluronic acid in tissue engineering, as a dermal filler and in osteoarthritis treatment. *Acta Biomater* **2013**, *9* (7), 7081-92. DOI: 10.1016/j.actbio.2013.03.005.

- 68. Szala, S.; Szary, J.; Cichoń, T.; Sochanik, A., Antiangiogenic gene therapy in inhibition of metastasis. *Acta Biochim Pol* **2002**, *49* (2), 313-21.
- 69. Rockwood, D. N.; Preda, R. C.; Yücel, T.; Wang, X.; Lovett, M. L.; Kaplan, D. L., Materials fabrication from Bombyx mori silk fibroin. *Nature Protocols* **2011**, *6* (10), 1612-1631. DOI: 10.1038/nprot.2011.379.
- 70. Waheed, A.; Mazumder, M. A. J.; Al-Ahmed, A.; Roy, P.; Ullah, N., Cell Encapsulation. In *Functional Biopolymers*, Jafar Mazumder, M. A.; Sheardown, H.; Al-Ahmed, A., Eds. Springer International Publishing: Cham, 2019; pp 377-427. DOI: 10.1007/978-3-319-95990-0 4.
- 71. Fischer, D.; Li, Y.; Ahlemeyer, B.; Krieglstein, J.; Kissel, T., In vitro cytotoxicity testing of polycations: influence of polymer structure on cell viability and hemolysis. *Biomaterials* **2003**, *24* (7), 1121-31. DOI: 10.1016/s0142-9612(02)00445-3.
- 72. Cao, Y.; Wang, B., Biodegradation of silk biomaterials. *Int J Mol Sci* **2009**, *10* (4), 1514-1524. DOI: 10.3390/ijms10041514.
- 73. Yao, X.; Zou, S.; Fan, S.; Niu, Q.; Zhang, Y., Bioinspired silk fibroin materials: From silk building blocks extraction and reconstruction to advanced biomedical applications. *Mater Today Bio* **2022**, *16*, 100381. DOI: 10.1016/j.mtbio.2022.100381.
- 74. Nicodemus, G. D.; Bryant, S. J., Cell encapsulation in biodegradable hydrogels for tissue engineering applications. *Tissue Eng Part B Rev* **2008**, *14* (2), 149-65. DOI: 10.1089/ten.teb.2007.0332.
- 75. Svaldo-Lanero, T.; Krol, S.; Magrassi, R.; Diaspro, A.; Rolandi, R.; Gliozzi, A.; Cavalleri, O., Morphology, mechanical properties and viability of encapsulated cells. *Ultramicroscopy* **2007**, *107* (10), 913-921. DOI: https://doi.org/10.1016/j.ultramic.2007.04.006.